Dual-Tracer PET/CT Protocol with [18F]-FDG and [68Ga]Ga-FAPI-46 for Cancer Imaging: A Proof of Concept

Katrin S. Roth[1], Conrad-Amadeus Voltin[1], Lutz van Heek[1], Simone Wegen[2], Klaus Schomäcker[1], Thomas Fischer[1], Simone Marnitz[2], Alexander Drzezga[1], and Carsten Kobe[1]

[1]Department of Nuclear Medicine, Faculty of Medicine, University Hospital Cologne, University of Cologne, Cologne, Germany; and [2]Department of Radiation Oncology, Cyberknife, and Radiotherapy, Faculty of Medicine, University Hospital Cologne, University of Cologne, Cologne, Germany

Imaging studies with PET tracers acting as fibroblast activation protein inhibitors (FAPIs) show promising results that could usefully complement [18F]-FDG in cancer imaging. **Methods:** All patients received [18F]-FDG PET/CT and dual-tracer PET/CT after an additional injection of [68Ga]Ga-FAPI-46 after the [18F]-FDG PET/CT. Two readers visually compared detection rate and analyzed target-to-background ratios for tumor and metastatic tissue in single- and dual-tracer PET/CT. **Results:** Detection rate in dual-tracer PET/CT was visually as good as that in single-tracer PET/CT in 4 patients and superior in 2 patients, whereas target-to-background ratios were significantly higher in dual-tracer PET/CT. **Conclusion:** Dual-tracer [18F]-FDG/[68Ga]Ga-FAPI-46 PET/CT within a single session is feasible and has potential. The dual-tracer approach may have superior sensitivity to [18F]-FDG PET/CT alone without compromising individual assessment of either scan.

Key Words: dual-tracer PET/CT; FDG; FAPI

Fibroblast activation protein (FAP) is a transmembrane glycoprotein expressed in tissue with activated stroma during wound healing and in chronically inflamed tissue (*1–3*). In vivo and histologic studies have shown that FAP is also expressed in the tumor microenvironment of human epithelial malignancies (*4,5*). Recent studies with quinolone-based PET radiotracers acting as FAP inhibitors (FAPIs) showed promising results for [68Ga]Ga-FAPI-46 PET/CT in cancer imaging (*5–7*). Previously suggested advantages of [68Ga]Ga-FAPI-46 PET/CT over [18F]-FDG PET/CT include fast tumor uptake (*8*) with a higher target-to-background ratio (TBR) (*9*). Low background uptake in most organs, including brain and liver, allows good detection of malignant lesions in these organs by [68Ga]Ga-FAPI-46 PET/CT (*10,11*).

Because our knowledge of the clinical impact of [68Ga]Ga-FAPI-46 is still incomplete, many therapy strategy decisions for various cancers are currently based on staging with [18F]-FDG PET/CT, representing the gold standard. Because of tumor heterogeneity, [68Ga]Ga-FAPI-46 PET/CT may not always represent the superior alternative; instead, the 2 tracers may provide complementary diagnostic information. [68Ga]Ga-FAPI-46 PET/CT would therefore often need to be run as a supplement to [18F]-FDG PET/CT to obtain comprehensive diagnostic information. The aim of the present study was to analyze the feasibility and impact of a single-session, dual-tracer PET/CT protocol for cancer staging in patients with head-and-neck tumors and esophageal cancer before radiotherapy.

TABLE 1
Patient Characteristics, Scan Data, and Lesion Detection with Single- vs. Dual-Tracer PET/CT

Characteristic	Mean	No. of patients	
		Single tracer	Dual tracer
Age (y)	72.5 ± 12.3		
Detected malignant findings on PET/CT			
Tumors (*n* = 7)			
Oropharyngeal cancer		2	2
Cancer of mouth floor		1	1
Esophageal cancer		4	4
Metastasis (*n* = 12)			
Lymph node metastasis			
Cervical		4	4
Mediastinal		1	2*
Mesenterial		1	1
Retroperitoneal		1	1
Parailiac		1	1
Pleural metastasis		1	1
Liver metastasis		1	1*
Adrenal gland metastasis		1	1
PET/CT			
Time between [68Ga]Ga-FAPI-46 injection and scan (min)	18.2 ± 20.1		
Time between [18F]-FDG and [68Ga]Ga-FAPI-46 scan (min)	81.3 ± 38.1		

*More metastases were detected in drainage area of mediastinal lymph nodes and liver on dual-tracer PET/CT than on single-tracer PET/CT.

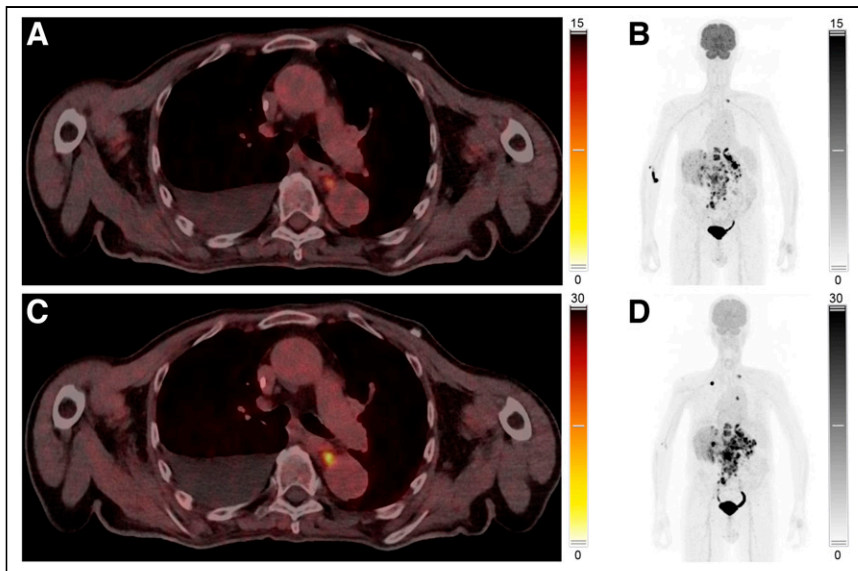**FIGURE 1.** (A) Axial single-tracer [^{18}F]-FDG PET/CT scan showing primary tumor at gastroesophageal junction and metastases in left adrenal gland and liver. (B) Maximum-intensity projection of single-tracer PET images displaying high uptake in brain tissue, tracer accumulation around injection site at right elbow, lymph node (LN) metastasis in left upper mediastinum, multiple abdominal LN metastases, and liver metastases. Additional benign accumulation of [^{18}F]-FDG is visible, caused by right-sided thoracolumbar osteoarthritis. (C) Transverse section of dual-tracer [^{18}F]-FDG/[^{68}Ga]Ga-FAPI-46 PET/CT scan of same patient as in A and B with mediastinal LN metastasis. (D) As all images were visually normalized to uptake in liver, maximum-intensity projection of dual-tracer PET/CT in same patient shows less pronounced tracer accumulation in brain tissue than does single-tracer PET/CT. In addition to lesions detected with single-tracer PET/CT, further abdominal LN metastasis and liver metastases are visualized via [^{18}F]-FDG/[^{68}Ga]Ga-FAPI-46 PET/CT. Focal tracer accumulation in right vein angle is due to intravenous tracer accumulation from former tracer depot at right elbow.

MATERIALS AND METHODS

Dual-Tracer Protocol

We developed a dual-tracer protocol consisting of an [^{18}F]-FDG PET/CT scan (injected activity, 272 ± 27.8 MBq; acquisition time, $81.3 \pm$ 38.1 min) and a subsequent repeat scan after injection of 177 ± 35.7 MBq of [^{68}Ga]Ga-FAPI-46 after 18.2 ± 20.1 min (Table 1). All patients received first the [^{18}F]-FDG PET/CT scan and then the dual-tracer PET/CT scan after an additional injection of [^{68}Ga]Ga-FAPI-46 immediately after the [^{18}F]-FDG PET/CT scan.

Patient Cohort

Images and data of 6 male patients who underwent both [^{18}F]-FDG PET/CT and dual-tracer PET/CT with [^{18}F]-FDG and [^{68}Ga]Ga-FAPI-46 between March and June 2021 were retrospectively analyzed. Their average age was 72.5 ± 12.3 y. All patients underwent imaging before radio-, chemo-, or immunotherapy. One patient had inoperable oropharyngeal carcinoma; 1 patient with oropharyngeal carcinoma had an additional floor-of-mouth cancer. Four patients had esophageal cancer (Table 1).

PET/CT Imaging and Interpretation

Two independent reviewers visually identified all pathologic findings on both single-tracer and dual-tracer PET/CT. The number of lesions and localizations were recorded and compared. CT scans were used for correlation and to exclude unspecific findings.

TBRs were obtained from both [^{18}F]-FDG PET/CT and combined [^{18}F]-FDG/[^{68}Ga]Ga-FAPI-46 PET/CT scans by determining ratios of count rates (CRs) between suggestive lesions and reference tissue. Maximum and peak CRs were obtained within tumor and metastatic lesions by drawing a spheric volume of interest around the lesion. Mean CRs within reference tissues were measured within a spheric volume of interest of 2-cm diameter in the right liver lobe and within a spheric volume of interest of 1-cm diameter in the cerebellum and mediastinal blood pool.

TABLE 2
TBRs of CRs Measured in Tumors, Metastasis, and Background on [^{18}F]-FDG/[^{68}Ga]Ga-FAPI-46 PET/CT and [^{18}F]-FDG PET/CT

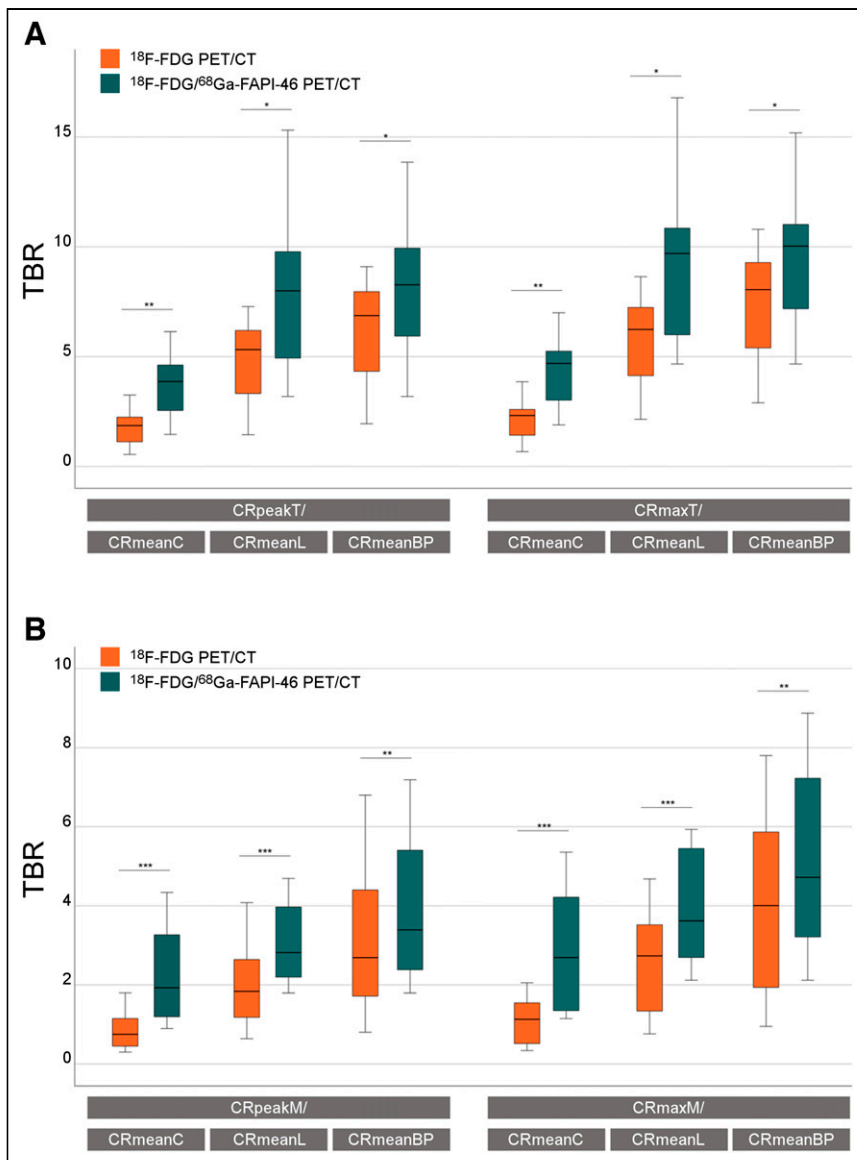| TBR	Dual tracer	Single tracer	Wilcoxon signed-rank test
CR tumor-to-background			
CR peak tumor/CR mean cerebellum	3.7 ± 1.7	1.8 ± 1.0	$z = -2.37, P = 0.008; r = 0.89$
CR peak tumor/CR mean liver	8.0 ± 4.1	4.7 ± 2.3	$z = -2.20, P = 0.016; r = 0.83$
CR peak tumor/CR mean mediastinal blood pool	8.2 ± 3.7	6.1 ± 2.8	$z = -2.20, P = 0.016; r = 0.83$
CR maximum tumor/CR mean cerebellum	4.3 ± 1.8	2.1 ± 1.1	$z = -2.37, P = 0.008; r = 0.89$
CR maximum tumor/CR mean liver	9.3 ± 4.2	5.7 ± 2.6	$z = -2.20, P = 0.016; r = 0.83$
CR maximum tumor/CR mean mediastinal blood pool	9.5 ± 3.7	7.3 ± 3.2	$z = -2.03, P = 0.023; r = 0.76$
CR metastasis-to-background			
CR peak metastasis/CR mean cerebellum	2.2 ± 1.2	0.8 ± 0.5	$z = -3.06, P \leq 0.001; r = 0.88$
CR peak metastasis/CR mean liver	2.9 ± 1.0	1.9 ± 1.0	$z = -3.06, P \leq 0.001; r = 0.88$
CR peak metastasis/CR mean mediastinal blood pool	3.9 ± 1.9	3.1 ± 1.8	$z = -2.51, P = 0.005; r = 0.72$
CR maximum metastasis/CR mean cerebellum	2.9 ± 1.6	1.1 ± 0.6	$z = -3.06, P \leq 0.001; r = 0.88$
CR maximum metastasis/CR mean liver	3.9 ± 1.4	2.5 ± 1.2	$z = -2.82, P \leq 0.001; r = 0.81$
CR maximum metastasis/CR mean mediastinal blood pool	5.2 ± 2.4	4.0 ± 2.2	$z = -2.35, P = 0.008; r = 0.68$

Data are mean $\pm$ SD.

RESULTS

Single-Tracer Versus Dual-Tracer Protocol

Both single- and dual-tracer PET/CT was tolerated well by all patients, without any recorded adverse reactions or side effects. All primary tumors could be clearly detected on [18F]-FDG PET/CT and [18F]-FDG/[68Ga]Ga-FAPI-46 PET/CT.

In 4 patients, cervical lymph node metastases were detected to an equal extent on single- and dual-tracer PET/CT (Table 1). In 1 patient, [18F]-FDG PET/CT revealed metastasis in only 1 mediastinal lymph node, whereas [18F]-FDG/[68Ga]Ga-FAPI-46 PET/CT showed tracer accumulation in 2 additional lymph nodes of the same drainage region. One mediastinal lymph node of a different patient displayed a discrete nonsuggestive tracer accumulation on [18F]-FDG PET/CT but a suspiciously high accumulation on [18F]-FDG/[68Ga]Ga-FAPI-46 PET/CT. [18F]-FDG PET/CT and [18F]-FDG/[68Ga]Ga-FAPI-46 PET/CT showed an equal extent of pleural metastasis in one patient and a metastasis in the adrenal gland of another patient. [18F]-FDG/[68Ga]Ga-FAPI-46 PET/CT displayed a higher number of liver metastases than did [18F]-FDG PET/CT ($n = 3$–5) in the patient with a metastasis in the adrenal gland (Fig. 1).

Whereas [18F]-FDG/[68Ga]Ga-FAPI-46 PET/CT imaging allowed detection of several additional suggestive lesions, no lesions detected on [18F]-FDG PET/CT were missed in the dual-tracer approach.

Higher Mean TBRs in Tumors and More Metastasis Shown on Dual- Than Single-Tracer PET/CT

As expected, TBRs between tumors and background tissue were consistently higher on combined [18F]-FDG/[68Ga]Ga-FAPI-46 PET/CT than on [18F]-FDG PET/CT alone (Table 2; Fig. 2). The TBRs measured by the Wilcoxon signed-rank test were significantly higher on [18F]-FDG/[68Ga]Ga-FAPI-46 PET/CT than on [18F]-FDG PET/CT ($z < -2$; $P = 0.023$–0.008), with a strong correlation ($r \geq 0.76$) (Table 2).

TBRs measured between metastases and background tissues were lower in general (Table 2) because of the lower CR of metastatic tissue. The Wilcoxon signed-rank test results were statistically significant ($z = -2.35$ to -3.06; $P \leq 0.008$), with a strong correlation ($r = 0.68$–0.88) (Table 2).

Unspecific Tracer Accumulation on Dual-Tracer PET/CT

Unspecific tracer accumulation was detected on dual-tracer PET/CT around the hip joint and intramuscularly in the flexors of the hip

FIGURE 2. Box plot of TBRs calculated from peak and maximum CR of tumors (CRpeakT and CRmaxT, respectively) (A) and peak and maximum CR of metastasis (CRpeakM and CRmaxM, respectively) (B) vs. mean CR of background cerebellum (CRmeanC), liver (CRmeanL), and mediastinal blood pool (CRmeanBP). Plots clearly display tendency of median TBRs to be higher on dual-tracer [18F]-FDG/[68Ga]Ga-FAPI-46 PET/CT than on single-tracer [18F]-FDG PET/CT. These results were most obvious in TBRs of malignant tissue with cerebellum or liver as background.

All procedures were performed according to the regulations of the local authorities (District Administration of Cologne, Germany) and after the local institutional review board (University of Cologne) approved the retrospective analysis. This retrospective study was performed in accordance with the Declaration of Helsinki, with the written consent of all patients to PET/CT imaging and inclusion of their data for scientific analysis.

Statistics

Descriptive statistics were used to present patient characteristics and results. A Wilcoxon matched-pairs signed-rank test was performed to check for significant differences between continuous variables. A P value of less than 0.05 was regarded as statistically significant. The Pearson correlation coefficient was used to measure

in 1 patient, evaluated as bursitis or tendinopathy. A pleural tracer accumulation was detected in a different patient, most probably caused by scar tissue. An unspecific tracer accumulation was seen in the right femoral head and in subcapsular regions of the left liver, most likely correlating with reactive processes. In 1 patient, unspecific tracer accumulation was seen in the vein angle (Fig. 1).

DISCUSSION

The present study compared dual $[^{18}F]$-FDG/$[^{68}Ga]$Ga-FAPI-46 PET/CT with single $[^{18}F]$-FDG PET/CT and demonstrated the feasibility and tolerability of dual-tracer PET/CT, as well as its potentially higher sensitivity in lesion detection.

Superior diagnostic performance of $[^{68}Ga]$Ga-FAPI-46 PET/CT compared with $[^{18}F]$-FDG PET/CT has been described recently and was attributed mainly to higher TBRs (9). We observed an equivalent performance in 4 patients and diagnostic superiority of $[^{18}F]$-FDG/$[^{68}Ga]$Ga-FAPI-46 PET/CT over $[^{18}F]$-FDG PET/CT in two.

By means of TBR, we showed that tracer accumulation was significantly higher on $[^{18}F]$-FDG/$[^{68}Ga]$Ga-FAPI-46 PET/CT than on $[^{18}F]$-FDG PET/CT in patients with head-and-neck tumors and esophageal cancer. Since the diagnostic performance of $[^{68}Ga]$Ga-FAPI-46 PET/CT has been shown to be best shortly after administration (12) and $[^{18}F]$-FDG PET/CT is currently the gold standard, we recommend the injection of $[^{68}Ga]$Ga-FAPI-46 as a second tracer after the $[^{18}F]$-FDG PET/CT scan.

The main aim of developing this dual-tracer protocol is better lesion detection with $[^{68}Ga]$Ga-FAPI-46 in less $[^{18}F]$-FDG–avid malignancies and a higher TBR due to accumulation of both tracers in the malignant lesions. Limitations of this approach could be the failure to define exclusively $[^{18}F]$-FDG–positive lesions, diminished high sensitivity of $[^{68}Ga]$Ga-FAPI-46–positive lesions in liver and brain hampered by $[^{18}F]$-FDG background, and loss of the ability to evaluate metabolic response since SUVs are not measurable. Because it has recently been shown that FAP can also be targeted with radioligand therapy in the animal model (13), the dual-tracer protocol would not allow safe detection of FAP expression as a theranostic approach.

In summary, the combined approach using 2 tracers for PET/CT imaging enables patients to undergo 2 PET/CT scans with consecutively higher sensitivity within the same medical appointment.

CONCLUSION

As demonstrated by visual and semiquantitative assessment, a single-session, dual-tracer protocol combining the strengths of 2 tracers is practicable, with no loss of diagnostic information relevant to cancer staging. We favor a protocol whereby standard $[^{18}F]$-FDG PET/CT is performed before the combined $[^{18}F]$-FDG/$[^{68}Ga]$Ga-FAPI-46 PET/CT within 1 appointment. Future studies may consider simultaneous injection of both tracers and acquisition of just a single scan, to further simplify the procedure.

DISCLOSURE

KEY POINTS

QUESTION: Is combined assessment of single-tracer $[^{18}F]$-FDG PET/CT and dual-tracer $[^{18}F]$-FDG/$[^{68}Ga]$Ga-FAPI-46 PET/CT within 1 appointment practical and feasible and have diagnostic sensitivity comparable to that of $[^{18}F]$-FDG PET/CT alone?

PERTINENT FINDINGS: Single- and dual-tracer PET/CT showed equal results in 4 patients, and lesion detection with dual-tracer PET/CT was superior in 2 patients. Semiquantitative analyses of TBRs were significantly higher in dual-tracer than single-tracer PET/CT scans.

IMPLICATIONS FOR PATIENT CARE: Proving the practicability of a single-session, dual-tracer protocol allows combining the strengths of 2 complementary tracers, with equal and in some cases superior diagnostic sensitivity for cancer staging.

REFERENCES

1. Mathew S, Scanlan MJ, Mohan Raj BK, et al. The gene for fibroblast activation protein alpha (FAP), a putative cell surface-bound serine protease expressed in cancer stroma and wound healing, maps to chromosome band 2q23. *Genomics*. 1995; 25:335–337.
2. Bauer S, Jendro MC, Wadle A, et al. Fibroblast activation protein is expressed by rheumatoid myofibroblast-like synoviocytes. *Arthritis Res Ther*. 2006;8:R171.
3. Wang XM, Yao TW, Nadvi NA, Osborne B, McCaughan GW, Gorrell MD. Fibroblast activation protein and chronic liver disease. *Front Biosci*. 2008;13: 3168–3180.
4. Garin-Chesa P, Old LJ, Rettig WJ. Cell surface glycoprotein of reactive stromal fibroblasts as a potential antibody target in human epithelial cancers. *Proc Natl Acad Sci USA*. 1990;87:7235–7239.
5. Kratochwil C, Flechsig P, Lindner T, et al. ^{68}Ga-FAPI PET/CT: tracer uptake in 28 different kinds of cancer. *J Nucl Med*. 2019;60:801–805.
6. Meyer C, Dahlbom M, Lindner T, et al. Radiation dosimetry and biodistribution of ^{68}Ga-FAPI-46 PET imaging in cancer patients. *J Nucl Med*. 2020;61:1171–1177.
7. Giesel FL, Kratochwil C, Lindner T, et al. ^{68}Ga-FAPI PET/CT: biodistribution and preliminary dosimetry estimate of 2 DOTA-containing FAP-targeting agents in patients with various cancers. *J Nucl Med*. 2019;60:386–391.
8. Ballal S, Yadav MP, Moon ES, et al. Biodistribution, pharmacokinetics, dosimetry of $[^{68}Ga]$Ga-DOTA.SA.FAPi, and the head-to-head comparison with $[^{18}F]$F-FDG PET/CT in patients with various cancers. *Eur J Nucl Med Mol Imaging*. 2021;48: 1915–1931.
9. Giesel FL, Kratochwil C, Schlittenhardt J, et al. Head-to-head intra-individual comparison of biodistribution and tumor uptake of ^{68}Ga-FAPI and ^{18}F-FDG PET/CT in cancer patients. *Eur J Nucl Med Mol Imaging*. 2021;48:4377–4385.
10. Windisch P, Röhrich M, Regnery S, et al. Fibroblast activation protein (FAP) SPECIFIC PET for advanced target volume delineation in glioblastoma. *Radiother Oncol*. 2020;150:159–163.
11. Shi X, Xing H, Yang X, et al. Fibroblast imaging of hepatic carcinoma with ^{68}Ga-FAPI-04 PET/CT: a pilot study in patients with suspected hepatic nodules. *Eur J Nucl Med Mol Imaging*. 2021;48:196–203.
12. Ferdinandus J, Kessler L, Hirmas N, et al. Equivalent tumor detection for early and late FAPI-46 PET acquisition. *Eur J Nucl Med Mol Imaging*. 2021;48: 3221–3227.
13. Watabe T, Liu Y, Kaneda-Nakashima K, et al. Theranostics targeting fibroblast activation protein in the tumor stroma: ^{64}Cu- and ^{225}Ac-labeled FAPI-04 in pancreatic cancer xenograft mouse models. *J Nucl Med*. 2020;61:563–569.